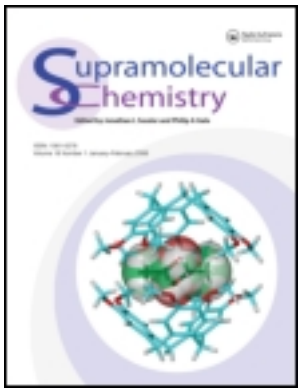

Supramolecular Chemistry
Publication details, including instructions for authors and subscription information:
http://www.tandfonline.com/loi/gsch20

Theoretical study of absorption spectrum of dirhodium tetracarboxylate complex $[Rh_2(CH_3COO)_4(H_2O)_2]$ in aqueous solution revisited

Yusuke Kataoka [a], Yasutaka Kitagawa [a], Toru Saito [a], Yasuyuki Nakanishi [a], Konomi Sato [b], Yuhei Miyazaki [b], Takashi Kawakami [a], Mitsutaka Okumura [a], Wasuke Mori [b] & Kizashi Yamaguchi [a]

[a] Department of Chemistry, Graduate school of Science, Osaka University, Toyonaka, Japan
[b] Department of Chemistry, Faculty of Science, Kanagawa University, Hiratsuka, Japan

Available online: 13 Apr 2011

To cite this article: Yusuke Kataoka, Yasutaka Kitagawa, Toru Saito, Yasuyuki Nakanishi, Konomi Sato, Yuhei Miyazaki, Takashi Kawakami, Mitsutaka Okumura, Wasuke Mori & Kizashi Yamaguchi (2011): Theoretical study of absorption spectrum of dirhodium tetracarboxylate complex $[Rh_2(CH_3COO)_4(H_2O)_2]$ in aqueous solution revisited, Supramolecular Chemistry, 23:03-04, 329-336

To link to this article: http://dx.doi.org/10.1080/10610278.2010.534553

Supramolecular Chemistry
Vol. 23, Nos. 3–4, March–April 2011, 329–336

Theoretical study of absorption spectrum of dirhodium tetracarboxylate complex $[Rh_2(CH_3COO)_4(H_2O)_2]$ in aqueous solution revisited

Yusuke Kataoka[a]*, Yasutaka Kitagawa[a], Toru Saito[a], Yasuyuki Nakanishi[a], Konomi Sato[b], Yuhei Miyazaki[b], Takashi Kawakami[a], Mitsutaka Okumura[a], Wasuke Mori[b] and Kizashi Yamaguchi[a]

[a]*Department of Chemistry, Graduate school of Science, Osaka University, Toyonaka, Japan;* [b]*Department of Chemistry, Faculty of Science, Kanagawa University, Hiratsuka, Japan*

(*Received 9 July 2010; final version received 20 October 2010*)

The electronic structures of ground and excited states of $[Rh_2(CH_3COO)_4(H_2O)_2]$ in aqueous solution are studied using a density functional theory (DFT) with a time-dependent (TD) method. Up to now, several theoretical assignments and explanations of its excitation characters have been reported based on the absorption spectra. In this study, we reinvestigate its absorption spectrum by the TD-DFT approach with the polarisable continuum model in order to clarify the excitation characters of the complex, especially in the aqueous solution well.

Keywords: absorption spectra; TD-DFT calculation; dirhodium tetracarboxylate; rhodium complex; paddle-wheel complex

1. Introduction

Dinuclear tetracarboxylates with a paddle-wheel molecular structure are the typical compounds that are widely utilised for the field of modern coordination chemistry. One of the most studied dinuclear paddle-wheel complex is dirhodium tetracarboxylate $[Rh_2(RCOO)_4(L)_2]$ (R = aromatic ring, alkyl chain, etc., L = solvent molecules), which has been applied for practical catalysts such as a carbenoid insert reaction, an olefin hydrogenation, a water splitting and so on (*1–3*). Another important aspect of the $[Rh_2(RCOO)_4(L)_2]$ complex is its ability to bind nucleic acids. For example, it is utilised as an inhibitor of DNA replication, and for a photocleavage of the DNA with a visible light (*4*). In addition, it is also reported that related dirhodium complexes can act as antibacterial agents and can exhibit a cytostatic activity against a human oral carcinoma (*5*).

On the other hand, photo-activated properties of supramolecular complexes based on the dirhodium paddle-wheel motif have also been explored since a long-lifetime transition of $[Rh_2(CH_3COO)_4(L)_2]$ species (ca. 3–5 μs) has been reported (*6*). So far, numerous studies of the absorption spectra of $[Rh_2(CH_3COO)_4(H_2O)_2]$ complex have been reported (Figure 1).

To the best of our knowledge, the first attempt to measure the absorption spectrum of $[Rh_2(CH_3COO)_4(L')_2]$ ($L' = H_2O, C_2H_5OH$, and so on) was by Johnson et al. (*7*) in 1963. From the measurements, they confirmed that $[Rh_2(CH_3COO)_4(L)_2]$ had two low-intensity bands (A-band and B-band) at 587 and 447 nm, respectively. After that, in 1970, Dubicki and Martin (*8*) reported the absorption spectrum of $[Rh_2(CH_3COO)_4(H_2O)_2]$ even at the UV region (~200 nm). In the study, they newly found a smooth shoulder (shoulder C) and an intense band (D-band) at around 250 and 220 nm, respectively. On the other hand, polarised spectra of single crystals of $[Rh_2(CH_3COO)_4(H_2O)_2]$ were measured by Martin et al. (*9*) at about 300 and 15 K in 1979. They reported that the A–B bands and shoulder C at 300 K appeared at 595, 400–476 (broad band) and 385 nm, respectively; however the blue shift occurred in the A–B bands, but not in shoulder C at 15 K. In 1984, Miskowski and co-workers (*10*) reinvestigated the polarised spectra of single crystals and also observed an absorption spectrum of $[Rh_2(CH_3COO)_4(H_2O)_2]_n$ in solutions. From the results, they reported that the maximum peaks and the molar absorption coefficients are 585 nm (A-band; $\varepsilon = 240$), 443 nm (B-band; $\varepsilon = 112$), 250 nm (shoulder C; $\varepsilon = 4000$) and 218.5 nm (D-band; $\varepsilon = 17{,}000$), respectively. In addition to those results, some studies about the absorption spectra of $[Rh_2(RCOO)_4(H_2O)_2]$ have also been reported (*11*). From all of these experimental studies, it is concluded that the absorption spectrum of the $[Rh_2(CH_3COO)_4(H_2O)_2]_n$ in the aqueous solutions has three intense bands and a smooth shoulder in the region of 200–800 nm.

On the other hand, several theoretical studies have also been devoted to clarifying the electronic structures and the absorption spectra of $[Rh_2(RCOO)_4(H_2O)_2]$. The first attempt to assign its transition character was presented by Dubicki and Martin (*8*). They applied the

*Corresponding author. Email: kataoka@chem.sci.osaka-u.ac.jp

ISSN 1061-0278 print/ISSN 1029-0478 online

DOI: 10.1080/10610278.2010.534553
http://www.informaworld.com

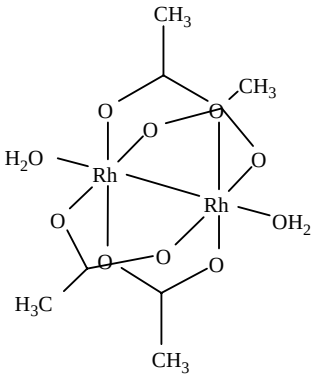

Figure 1. Molecular structure of $[Rh_2(CH_3COO)_4(H_2O)_2]$.

SCCC-molecular orbitals (MO) calculations to the $[Rh_2(CH_3COO)_4(H_2O)_2]$ complex. The results indicated that the dominant excitation characters of each bands and shoulder were as follows: A-band; $Rh_2(\pi*) \rightarrow Rh_2(\sigma*)$, B-band; $Rh_2(\pi) \rightarrow Rh_2(\sigma*)$, shoulder C; $Rh_2(\sigma) \rightarrow Rh_2(\sigma*)$ and D-band; $Rh_2(\sigma) \rightarrow Rh_2(\sigma*)$. After that, the SCF-Xα-SW calculations were performed by Norman and Kolari (*12*) in 1978. Their results revised the assignment of dominant excitation characters, i.e. B-band and D-band are $Rh_2(\pi*) \rightarrow Rh_2(\sigma*)$—O (charge transfer (CT)) and $Rh_2(\sigma)$-HCOO $\rightarrow Rh_2(\sigma*)$ (CT), respectively. At present, almost all of experimental chemists referred this assignment for the excitation characters of the novel dirhodium tetracarboxylate complexes. While, in 1996, Stranger and co-workers (*13*) performed Xα-SW MO calculations on $[Rh_2(HCOO)_4(H_2O)_2]$, and they also proposed another assignments of excitation characters of shoulder C and the D-band. They suggested that shoulder C mainly came from an $Rh_2(\sigma) \rightarrow Rh_2(\sigma*)$ transition with a minor H_2O or a HCOO $\rightarrow Rh_2(\sigma*)$—O transition and the D-band originated in an $Rh_2(\pi*) \rightarrow Rh_2(\sigma*)$—O CT with a minor H_2O or HCOO $\rightarrow Rh_2(\sigma*)$—O transition. Recently, in order to clarify the electronic structure and the absorption spectrum of $[Rh_2(CH_3COO)_4(H_2O)_2]$ well, Sizova and Ivanova reported the results of the time dependent-density functional theory (TD-DFT) calculations (B3LYP/ LANL2DZ and 6-31G** level) of $[Rh_2(HCOO)_4(H_2O)_2]$ in a gas phase condition (*14*, *15*). In the paper, they optimised a geometry of $[Rh_2(HCOO)_4(H_2O)_2]$, but the obtained Rh—Rh distance (2.465 Å) significantly overestimated the experimental one (2.386 Å). In addition, the calculated excitation energies showed red shifts in comparison with experimental values, and the assignments of excitations in the UV region were not clear. Thus, as mentioned above, the absorption spectra of the dirhodium tetra-acetato complexes still have not been clarified yet. Therefore, it is meaningful to explain the excited states of the dirhodium acetato complexes by theoretical calculations, because it is necessary for the further understanding of their properties and the creation of the novel photo-functional supramolecular complex or medicine.

On the basis of the background mentioned above, in this study, we reinvestigate the ground and the low-lying excited states of $[Rh_2(RCOO)_4(H_2O)_2]$ in aqueous solution using the DFT method to understand the optical absorption properties. The ground state was calculated by B3LYP method, while the TD method was applied for the excitation. The optimised structure was discussed in comparison with the experimental X-ray (crystal) structure and the previously reported optimised structures. In addition, we also examined a dependency of the calculated excitation characters on basis sets.

2. Theoretical and experimental methods

2.1 Computational details

All calculations in this paper were performed by the Gaussian 09 program package (*16*). In order to consider the basis set dependency, we optimised the geometrical structures of $[Rh_2(CH_3COO)_4(H_2O)_2]$ for the ground state with three different basis sets (**B1**: LANL2DZ for Rh, 6-31G** for others, **B2**: LANL2DZ for Rh, 6-31++G** for others and **B3**: DZVP for Rh, 6-31G** for others), without any symmetry constraints. As it is well known, the LANL2DZ, which is a split-valence double-ζ basis set introduces the effective pseudo-potentials that approximate the potential of the nucleus and core electrons for the valence electrons in order to reduce the computational costs. On the other hand, the DZVP is an all-electron basis set consisting of a double-ζ valence plus polarisation functions. The optimised structures have no negative frequencies.

For the excited states calculations, we used the TD-DFT method that is widely used for excited state calculations because of its reasonable accuracy and low computational cost. The much accurate *ab initio* wave function methods such as SAC-CI, EOM-CC, MR-CI and CAS-PT2 were not examined due to their large computational costs. In the TD-DFT calculations, it is reported that the functionals including 20–25% Hartree–Fock (HF) exchange provide good calculated results that are in agreement with the experimental absorption spectra (*17*). Therefore, in this study, B3LYP (including 20% HF exchange) was used for all calculations. Since there are few reports about the open-shell singlet calculations on $[Rh_2(RCOO)_4L_2]$, we, first, applied a spin-unrestricted open-shell calculation with U-B3LYP/LANL2DZ/6-31++G** for $[Rh_2(CH_3COO)_4(H_2O)_2]$. However, the calculated wave function converged to a closed-shell electronic structure, nevertheless we used the open-shell singlet wave function as an initial electronic structure. Therefore, a spin-restricted method was employed for all the calculations. The TD-DFT excitation energies and

Table 1. Structural parameters, bond lengths (Å) and dihedral angles (°) of $[Rh_2(CH_3COO)_4(H_2O)_2]$.

Basis sets	**B1**	**B2**	**B3**	Exp.
Rh—Rh	2.409	2.415	2.413	2.386
Rh—O (bridge)	2.077	2.077–2.079	2.086–2.090	2.042
Rh—OH_2 (axial)	2.407	2.405	2.408	2.309
RhRhO (bridge)	87.4	87.4	87.3	87.7
RhRhO (axial)	172.7	174.7, 174.9	172.0, 172.1	176.5

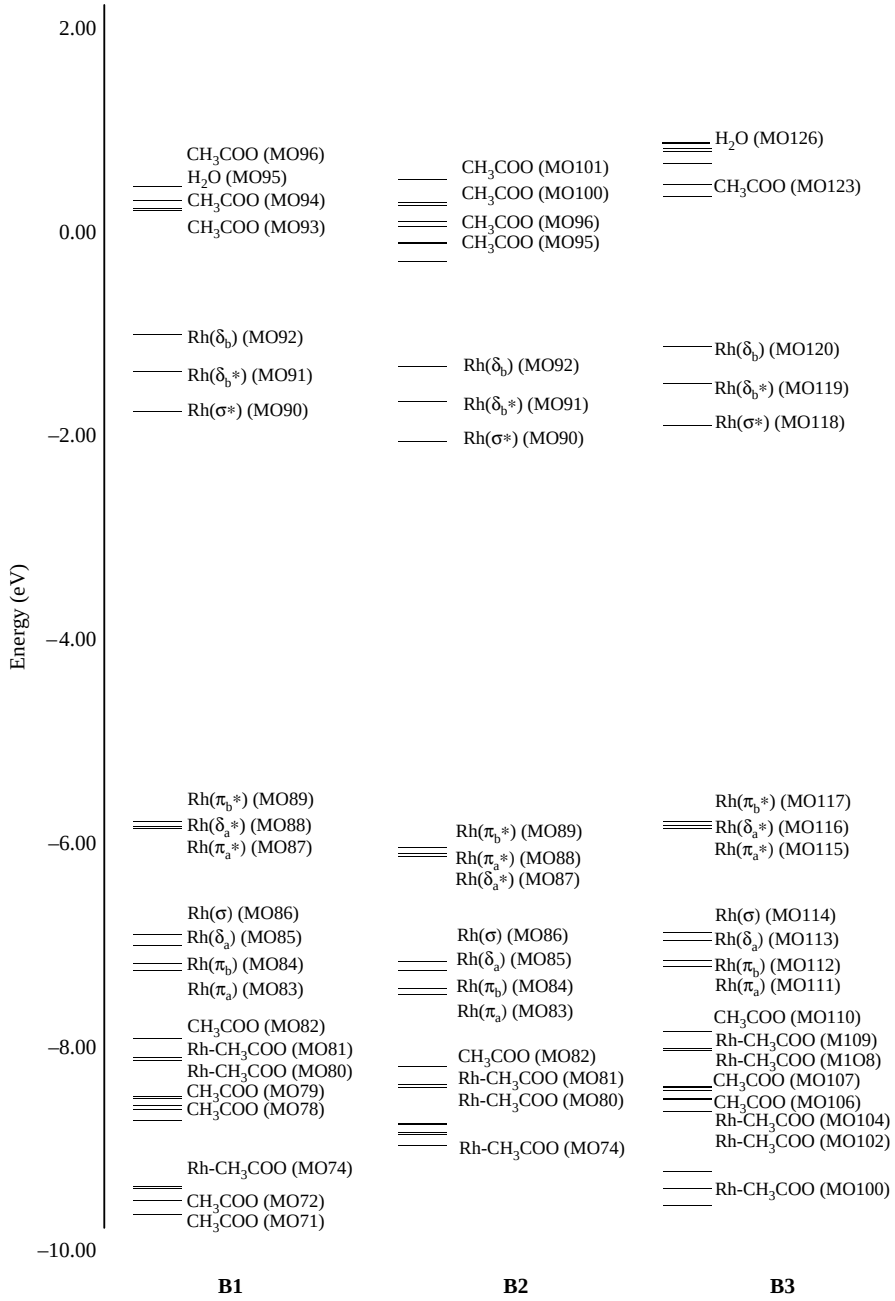

Figure 2. Molecular orbital diagrams of $[Rh_2(CH_3COO)_4(H_2O)_2]$ calculated with **B1**–**B3** basis sets.

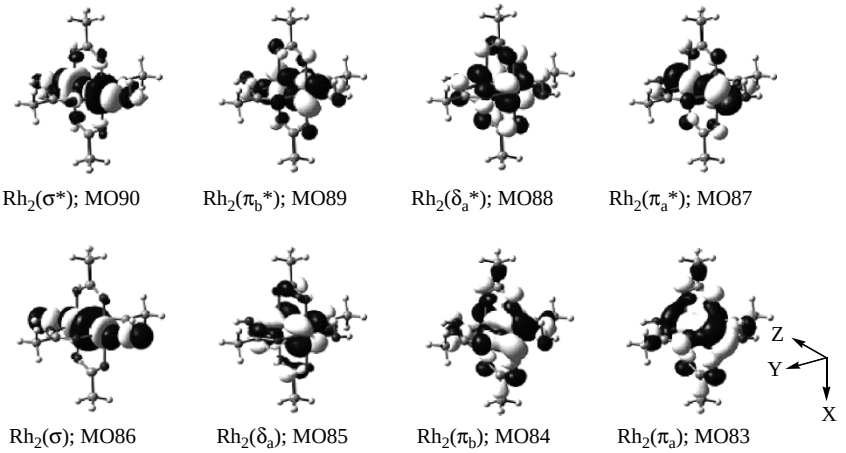

Figure 3. Molecular orbital (MO83–90) of $[Rh_2(CH_3COO)_4(H_2O)_2]$ calculated with the **B1** basis set.

oscillator strengths were checked for the 65 lowest spin-allowed singlet–singlet excitations, up to 200.0 nm. The effect of the H_2O solution in the TD-DFT calculations was taken by the non-equilibrium version of the conductor-like polarisable continuum model (C-PCM). The calculated absorption energies and intensities were depicted by a Gaussian function, in which the half-height bandwidth was 0.25 eV on the GaussView 4 program.

2.2 Experimental absorption spectrum of $Rh_2(CH_3COO)_4(H_2O)_2$

As mentioned above, the experimental absorption spectra of $[Rh_2(CH_3COO)_4(H_2O)_2]$ were energetically investigated in the 1970–1980s. However, in order to reconfirm the spectra, we experimentally measured the absorption spectrum of $[Rh_2(CH_3COO)_4(H_2O)_2]$ in aqueous solution, again. A sample material of $[Rh_2(CH_3COO)_4(H_2O)_2]$ was obtained commercially from Wako Co. and was used without further purification. The UV–vis spectrum was measured by a JASCO V-660 spectrophotometer at 300 K.

3. Results and discussion

3.1 Optimised geometry of $[Rh_2(CH_3COO)_4(H_2O)_2]$

At first, we carried out geometry optimisation of $[Rh_2(CH_3COO)_4(H_2O)_2]$ with the different three basis sets (**B1**–**B3**). Some important optimised parameters are summarised in Table 1, together with the X-ray data. As summarised in Table 1, the optimised bond lengths and bond angles are hardly changed by the basis sets (**B1**–**B3**) and are in good agreement with the experimental values, except for the Rh—OH_2 length. For example, the calculated Rh—Rh bond lengths are almost equal to the experimental value (within 0.029 Å), although the calculated Rh—OH_2 lengths are slightly overestimated (about 0.1 Å). The difference in the Rh—OH_2 length between the calculation and the X-ray is considered to originate from the effects of crystal packing.

As mentioned above, Sizova and Ivanova have reported the calculated results of $[Rh_2(HCOO)_4(H_2O)_2]$ with B3LYP/LANL2DZ/6-31G**. In that article, they described that the optimised Rh—Rh and Rh—OH_2 lengths were 2.465 and 2.307 Å, respectively. In order to explain the difference between their results and ours, we carried out the frequency calculations with both structures. The results indicate that the reported geometry involves the negative frequency as summarised in Table S1 in the supporting information available online, suggesting that their structure is not a global minimum. From those points of view, we use our optimised geometry for the further calculations explained below.

3.2 Electronic structures of $Rh_2(CH_3COO)_4(H_2O)_2$ in aqueous solution

In order to consider the MOs concerning the absorption spectrum in aqueous solution, the orbital energies around the valence orbitals are depicted in Figure 2. And the MOs calculated by the **B1** basis set are also shown in Figure 3.

In the case of **B1** basis sets, orbitals from HOMO-6 to HOMO are almost localised around the Rh_2 unit, and the orbital order becomes $\pi_a^2\pi_b^2\delta^2\sigma^2\pi_a{*}^2\delta{*}^2\pi_b{*}^2$. The virtual orbitals from LUMO to LUMO + 2 that are σ*, δ_b*, and δ_b, respectively, are also localised on the Rh_2 unit. As shown in Figure 2, the order and energies of the valence orbitals (HOMO-6 to LUMO + 2) calculated by **B3** basis set are similar to the results of the **B1** basis set, although a HOMO–LUMO gap is rather small. On the other hand, the **B2** basis set, which involves diffuse functions, makes orbital energies lower in all orbitals, and the orbital order is slightly altered.

Table 2. Calculated excitation energies, oscillator strengths (f), excitation assignments and their expansion coefficients of $[Rh_2(CH_3COO)_4(H_2O)_2]$ in visible light region.

Basis sets	State	E/nm (eV)	Oscillator (f)	Assignment and expansion coefficient
B1	S1	585.5 (2.12)	0.0035	$Rh_2(\pi_b*) \rightarrow Rh_2(\sigma*)$ (0.649), $Rh_2(\pi_a*) \rightarrow Rh_2(\delta_b*)$ (0.198)
	S2	574.5 (2.16)	0.0028	$Rh_2(\pi_a*) \rightarrow Rh_2(\sigma*)$ (0.644), $Rh_2(\pi_b*) \rightarrow Rh_2(\delta_b*)$ (0.224)
	S3	438.3 (2.83)	0.0014	$Rh_2(\pi_b*) \rightarrow Rh_2(\delta_b*)$ (0.606)
	S4	430.5 (2.88)	0.0016	$Rh_2(\pi_a*) \rightarrow Rh_2(\delta_b*)$ (0.615)
B2	S1	597.1 (2.08)	0.0035	$Rh_2(\pi_b*) \rightarrow Rh_2(\sigma*)$ (0.649), $Rh_2(\pi_a*) \rightarrow Rh_2(\delta_b*)$ (0.201)
	S2	586.0 (2.12)	0.0030	$Rh_2(\pi_a*) \rightarrow Rh_2(\sigma*)$ (0.644), $Rh_2(\pi_b*) \rightarrow Rh_2(\delta_b*)$ (0.226)
	S3	444.3 (2.79)	0.0017	$Rh_2(\pi_b*) \rightarrow Rh_2(\delta_b*)$ (0.605)
	S4	437.0 (2.84)	0.0021	$Rh_2(\pi_a*) \rightarrow Rh_2(\delta_b*)$ (0.614)
B3	S1	625.6 (1.98)	0.0032	$Rh_2(\pi_b*) \rightarrow Rh_2(\sigma*)$ (0.671), $Rh_2(\pi_a*) \rightarrow Rh_2(\delta_b*)$ (0.181)
	S2	612.3 (2.03)	0.0025	$Rh_2(\pi_a*) \rightarrow Rh_2(\sigma*)$ (0.644), $Rh_2(\pi_b*) \rightarrow Rh_2(\delta_b*)$ (0.209)
	S3	458.8 (2.70)	0.0015	$Rh_2(\pi_b*) \rightarrow Rh_2(\delta_b*)$ (0.656)
	S4	449.7 (2.76)	0.0017	$Rh_2(\pi_a*) \rightarrow Rh_2(\delta_b*)$ (0.664)

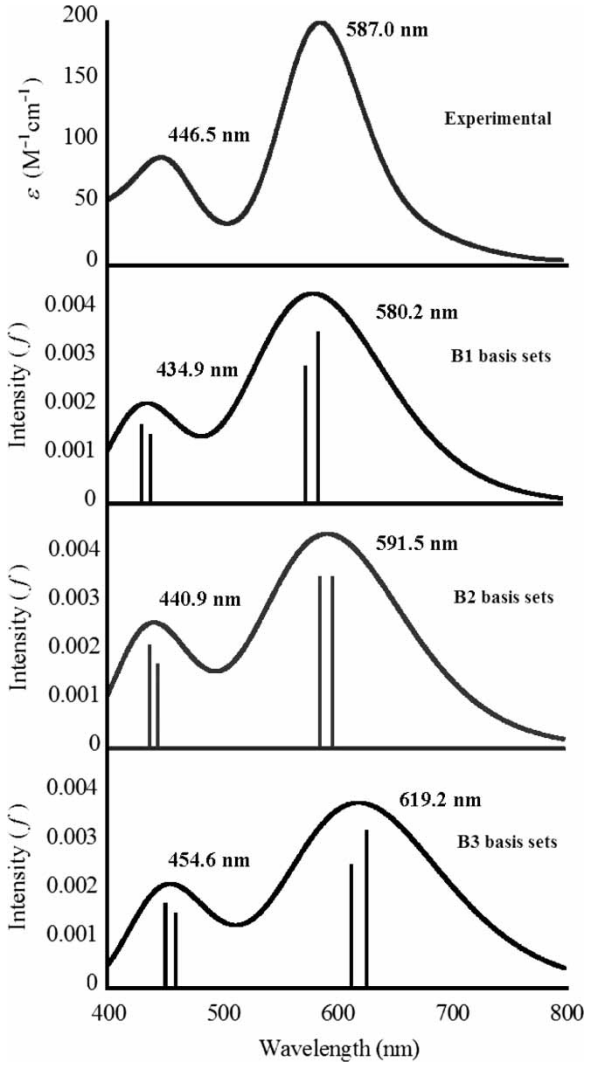

Figure 4. Experimental and theoretical absorption spectra of $[Rh_2(CH_3COO)_4(H_2O)_2]$ in the visible light region.

In order to investigate the basis set dependency on the metal charges, we calculated the Mulliken atomic populations of the Rh_2 unit. The calculated Mulliken atomic charge populations of the Rh_2 unit with **B1**–**B3** basis sets were 0.852, 0.712 and 0.901, respectively. These values indicated that the atomic charges of the Rh_2 unit calculated with **B1** and **B3** basis sets are almost equal. In other words, the ECP of the Rh ions does not affect the metal charges. On the other hand, the diffuse function in the basis set obviously influences the charges of Rh_2 units.

3.3 Theoretical assignment of absorption spectrum of $Rh_2(CH_3COO)_4(H_2O)_2$ in aqueous solution

Calculated excitation energies and oscillator strengths within the visible light region are summarised in Table 2. The experimental and simulated spectra are also shown in Figure 4. From these results, we find that the experimental spectrum shows two main bands at approximately 587.0 (A-band) and 446.5 nm (B-band) with molar coefficient values (ε) of 197.4 and 87.4 $M^{-1}\,cm^{-1}$, respectively. These peak positions are in good agreement with the experimental work of Johnson et al. (587 and 447 nm), although the molar absorption coefficients are relatively small.

As shown in Figure 4, the simulated spectra reproduce the experimental peak positions well. In all calculations, the four dominant transitions (S1–S4) are found in this region. In addition, the oscillator strengths and coefficients of the orbitals are quite similar to each other. The A-band in the simulated spectrum is dominantly constructed by S1 and S2 transitions. The lowest energy transition S1 is composed of $Rh_2(\pi_b*) \rightarrow Rh(\sigma*)$ (dominant) and Rh $(\pi_a*) \rightarrow Rh(\delta_b-*)$ (minor) transitions. On the other hand, the second transition S2 is described by $Rh_2(\pi_a*) \rightarrow Rh_2(\sigma*)$ (dominant) and $Rh_2(\pi_b*) \rightarrow Rh_2(\delta_b*)$ (minor) transitions. The B-band in the simulated spectrum involves the two major transitions (S3 and S4) that are Rh_2 $(\pi_a*) \rightarrow Rh_2(\delta_a*)$ and $Rh_2(\pi_a*) \rightarrow Rh_2(\delta_b*)$, respectively.

Table 3. Calculated excitation energies, oscillator strengths (*f*), excitation assignments and their expansion coefficients of $[Rh_2(CH_3COO)_4(H_2O)_2]$ in the UV region (Here, CH_3COO═OAc.)

Basis sets	State	E/nm (eV)	Oscillator (*f*)	Assignment
B1	S5	257.4 (4.82)	0.1638	$Rh_2(\sigma) \rightarrow Rh_2(\sigma^*)$ (0.535), $Rh_2(\delta_a^*) \rightarrow$ OAc (0.324), OAc $\rightarrow Rh_2(\sigma^*)$ (0.105)
	S6	252.2 (4.92)	0.0131	$Rh_2(\pi_b) \rightarrow Rh_2(\delta_b)$ (0.644), $Rh_2(\pi_b^*) \rightarrow Rh_2(\delta_b^*)$ (0.165)
	S7	249.3 (4.97)	0.0124	$Rh_2(\pi_a) \rightarrow Rh_2(\delta_b)$ (0.636), Rh—OAc $\rightarrow Rh_2(\sigma^*)$ (0.158)
	S8	233.6 (5.31)	0.0149	Rh—OAc $\rightarrow Rh_2(\sigma^*)$ (0.656)
	S9	232.7 (5.33)	0.0129	Rh—OAc $\rightarrow Rh_2(\sigma^*)$ (0.662)
	S10	221.6 (5.59)	0.1122	$Rh_2(\delta_a^*) \rightarrow$ OAc (0.597), Rh—OAc $\rightarrow Rh_2(\delta_b^*)$ (0.159), Rh—OAc $\rightarrow Rh_2(\delta_b)$ (0.140)
	S11	212.7 (5.83)	0.0799	Rh—OAc $\rightarrow Rh_2(\delta_b^*)$ (0.596), Rh—OAc $\rightarrow Rh_2(\sigma^*)$ (0.131)
	S12	211.8 (5.85)	0.0750	Rh—OAc $\rightarrow Rh_2(\delta_b^*)$ (0.579), OAc $\rightarrow Rh_2(\delta_b^*)$ (0.319), Rh—OAc $\rightarrow Rh_2(\sigma^*)$ (0.116)
	S13	204.5 (6.06)	0.0428	OAc $\rightarrow Rh_2(\delta_b^*)$ (0.571), Rh—OAc $\rightarrow Rh_2(\delta_b^*)$ (0.210), $Rh_2(\delta_a) \rightarrow$ OAc (0.117)
	S14	204.3 (6.07)	0.0597	OAc $\rightarrow Rh_2(\delta_b^*)$ (0.596)
B2	S5	260.3 (4.76)	0.1768	$Rh_2(\sigma) \rightarrow Rh_2(\sigma^*)$ (0.536), Rh—OAc $\rightarrow Rh_2(\delta_b)$ (0.112)
	S6	255.1 (4.86)	0.0161	$Rh_2(\pi_b) \rightarrow Rh_2(\delta_b)$ (0.647), Rh—OAc $\rightarrow Rh_2(\sigma^*)$ (0.121)
	S7	252.3 (4.91)	0.0150	$Rh_2(\pi_a) \rightarrow Rh_2(\delta_b)$ (0.641), Rh—OAc $\rightarrow Rh_2(\sigma^*)$ (0.142)
	S8	235.0 (5.28)	0.0200	Rh—OAc $\rightarrow Rh_2(\sigma^*)$ (0.664)
	S9	234.2 (5.29)	0.0174	Rh—OAc $\rightarrow Rh_2(\sigma^*)$ (0.668)
	S10	224.9 (5.51)	0.1334	$Rh(\delta_a^*) \rightarrow$ Rh—OAc (0.594), Rh $(\sigma) \rightarrow Rh_2(\sigma^*)$ (0.199), Rh—OAc $\rightarrow Rh_2(\delta_b)$ (0.137)
	S11	214.0 (5.79)	0.0976	Rh—OAc $\rightarrow Rh_2(\delta_b^*)$ (0.583), $Rh(\pi_a^*) \rightarrow$ OAc (0.199), Rh—OAc $\rightarrow Rh_2(\sigma^*)$ (0.118)
	S12	213.1 (5.81)	0.1000	Rh—OAc $\rightarrow Rh_2(\delta_b^*)$ (0.598), Rh—OAc $\rightarrow Rh_2(\sigma^*)$ (0.111)
	S13	205.8 (6.03)	0.0518	OAc $\rightarrow Rh_2(\delta_b^*)$ (0.636), Rh—OAc $\rightarrow Rh_2(\delta_b^*)$ (0.206)
	S14	205.4 (6.04)	0.0287	$Rh(\delta_a^*) \rightarrow$ OAc (0.504), $Rh(\delta_a^*) \rightarrow$ OAc (0.105)
B3	S5	265.3 (4.67)	0.1428	$Rh_2(\sigma) \rightarrow Rh_2(\sigma^*)$ (0.601), $Rh(\delta_a^*) \rightarrow$ OAc (0.272)
	S6	260.3 (4.76)	0.0101	$Rh_2(\pi_b) \rightarrow Rh_2(\delta_b)$ (0.648), $Rh(\pi_b^*) \rightarrow Rh_2(\delta_b^*)$ (0.152)
	S7	257.4 (4.82)	0.0089	$Rh_2(\pi_a) \rightarrow Rh_2(\delta_b)$ (0.636), $Rh(\pi_a^*) \rightarrow Rh_2(\delta^*)$ (0.154), Rh—OAc $\rightarrow Rh_2(\delta_b)$ (0.130)
	S8	244.4 (5.07)	0.0190	Rh—OAc $\rightarrow Rh_2(\sigma^*)$ (0.654), $Rh_2(\pi_a) \rightarrow Rh_2(\delta_b)$ (0.153)
	S9	244.1 (5.08)	0.0173	Rh—OAc $\rightarrow Rh_2(\sigma^*)$ (0.663), $Rh_2(\pi_b) \rightarrow Rh_2(\delta_b)$ (0.118)
	S10	222.7 (5.57)	0.0707	$Rh_2(\delta_b^*) \rightarrow$ OAc (0.624), Rh—OAc $\rightarrow Rh_2(\delta_b^*)$ (0.147), Rh—OAc $\rightarrow Rh_2(\delta_b)$ (0.138)
	S11	220.1 (5.63)	0.0926	Rh—OAc $\rightarrow Rh_2(\delta_b^*)$ (0.606), OAc $\rightarrow Rh_2(\delta_b^*)$ (0.283), Rh—OAc $\rightarrow Rh_2(\sigma^*)$ (0.129)
	S12	219.4 (5.65)	0.0830	Rh—OAc $\rightarrow Rh_2(\delta_b^*)$ (0.565), OAc $\rightarrow Rh_2(\delta_b^*)$ (0.297), OAc $\rightarrow Rh_2(\delta_b)$ (0.184)
	S13	212.0 (5.85)	0.0246	$Rh(\pi_a^*) \rightarrow H_2O$ (0.483), OAc $\rightarrow Rh_2(\delta_b^*)$ (0.481)
	S14	210.8 (5.88)	0.0781	OAc $\rightarrow Rh_2(\delta_b^*)$ (0.579)

Therefore, both A- and B-bands are considered to be simple d–d transitions from $Rh_2(\pi^*)$ orbitals. This assignment of A-band is same as that of the previous reports by Huckel and Xα-SW methods, while the B-band is not. The dominant transition characters reported by Sizova are the same as that of our results; however, the excitation energies and oscillator strengths are rather different.

We also examined the basis set dependency in transition character. The calculated excitation energies with the LANL2DZ basis set (**B1** and **B2**) tend to be in good agreement with the experimental values, while the values by the DZVP basis set (**B3**) seem to show a red shift of about 20–40 nm. The diffuse functions in the basis set do not change the spectrum drastically however, excitation energies calculated by the **B2** basis set slightly exhibits a red shift because of a decrease in HOMO–LUMO gap. As a result, the calculated peak positions by the **B2** basis set are the best in comparison with the experimental spectrum within the visible light region.

Next, the calculated excitation energies and the oscillator strengths in the UV light region are summarised in Table 3. The experimental and simulated spectra in the UV region are also shown in Figure 5. As shown in Figure 5, the experimental spectrum has a smooth shoulder C (245.5 nm; $\varepsilon = 3257.7$) and a high-energy D-band (218.9 nm; $\varepsilon = 13023.6$) as described in previous reports.

The peak positions of simulated spectra are also in good agreement with the experiment, although the intensities of the shoulder C are overestimated. This phenomenon that the TD-DFT has a difficulty in expressing a broad peak has already been reported by Tozer et al (*18*). Calculated results indicate that shoulder C consists of many transitions with similar oscillator strengths but, they have obviously different intensities. From the calculated results in Table 3, the $Rh_2(\sigma) \rightarrow Rh_2(\sigma_*)$ transition is dominant in shoulder C. However, the minor transitions around the dominant transition are changed by basis sets. The more intense high-energy absorption band, i.e. D-band is attributed to a number of d–d transitions and CT such as metal-to-ligand CT and ligand-to-metal CT.

About the basis set dependency on the transition character in the UV region, we cannot find significant difference in the calculated peak positions and their transition characters between the **B1** and **B2** basis sets,

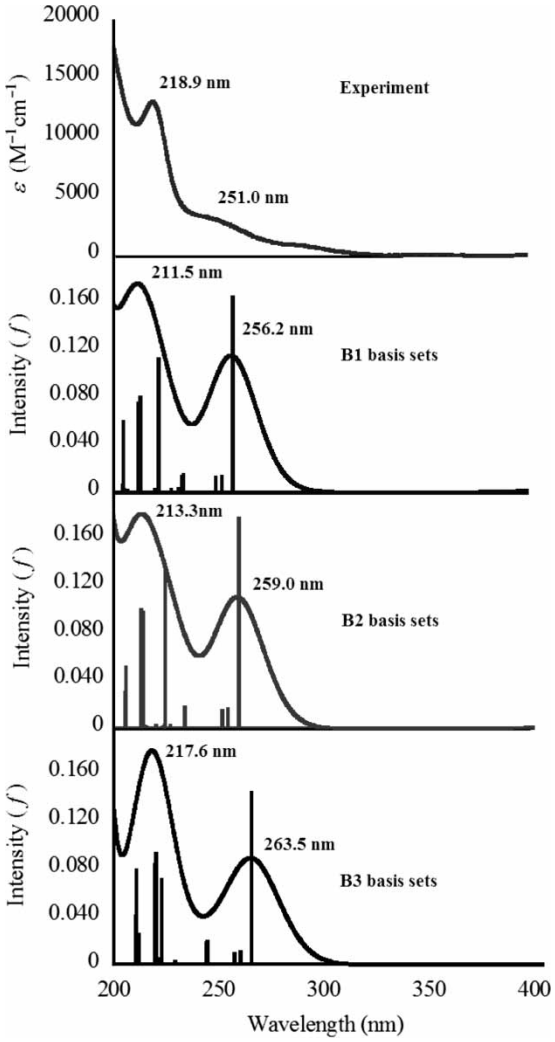

Figure 5. Experimental and theoretical absorption spectra of $[Rh_2(CH_3COO)_4(H_2O)_2]$ in the UV region.

suggesting that the effect of the diffuse functions is not large even in the UV region. However, the peak positions calculated by the **B3** basis set are completely different from those of **B1** and **B2** basis sets. These results indicate that the excitation characters of $[Rh_2(CH_3COO)_4(H_2O)_2]$ in the UV region are easily changed by the basis set for the Rh ions, but more applications and examples are needed to conclude which is the best for this system.

4. Conclusion

In this study, we revisited the absorption spectrum of the typical dirhodium tetracarboxylate complex, i.e. $[Rh_2(CH_3COO)_4(H_2O)_2]$ by the TD-DFT calculations, together with the PCM method. The two low-intensity transition bands (A- and B-bands) in the visible light region were simple d–d transitions from $Rh_2(d\pi*)$ orbital to $Rh_2(d\sigma*)$ and $Rh_2(d\delta*)$ orbitals. From the calculated oscillator strengths, the $Rh_2(\sigma) \rightarrow Rh_2(\sigma*)$ transition was considered to be the dominant component of shoulder C. In addition, the more intense high-energy D-band consists of a number of d–d and CT transitions. The dependency of basis sets on the transition property was also examined. The results indicated that the ECP of Rh ions affect the transition character in the UV region, but the diffuse functions obviously do not show influence in both visible and UV regions.

Acknowledgements

One of the authors (Y. Kataoka) expresses his special thanks to the Global COE (centre of excellence) Program 'Global Education and Research Center for Bio-Environmental Chemistry' of Osaka University. This work was supported by Grants-in-Aid for Scientific Research (KAKENHI)(Nos. 19750046, 19350070) from the Japan Society for the Promotion of Science (JSPS) and Grant-in-Aid for Scientific Research on Innovative Areas ('Coordination Programming' area 2170, No. 22108515) from the Ministry of Education, Culture, Sports, Science and Technology (MEXT).

References

(1) Hansen, J.; Davis, H.M.L. *Coord. Chem. Rev.* **2008**, *252*, 545–555.
(2) Naito, S.; Tanibe, T.; Saito, E.; Miyao, T.; Mori, W. *Chem. Lett.* **2001**, *30*, 1178–1179.
(3) Kataoka, Y.; Sato, K.; Miyazaki, Y.; Suzuki, Y.; Tanaka, H.; Kitagawa, Y.; Kawakami, T.; Okumura, M.; Mori, W. *Chem. Lett.* **2010**, *39*, 358–359.
(4) Fu, P.K.-L.; Bradley, P.M.; Turro, C. *Inorg. Chem.* **2001**, *40*, 2476–2477.
(5) Bien, M.; Pruchnik, F.P.; Seniuk, A.; Lachowicz, T.M.; Jakimowicz, P. *J. Inorg. Biochem.* **1999**, *73*, 49–55.
(6) Bradley, P.M.; Bursten, B.E.; Turro, C. *Inorg. Chem.* **2001**, *40*, 1376–1379.
(7) Johnson, S.A.; Hunt, H.R.; Neumann, H.M. *Inorg. Chem.* **1963**, *2*, 960–962.
(8) Dubicki, L.; Martin, R.T. *Inorg. Chem.* **1970**, *9*, 673–675.
(9) Martin, D.S.; Webb, T.R.; Robbins, G.A,; Fanwick, P.E. *Inorg. Chem.* **1979**, *18*, 475–478.
(10) Miskowski, V.M.; Schaefer, W.P.; Sadeghi, B.; Santarsiero, R.D.; Gray, H.B, *Inorg. Chem.* **1984**, *23*, 1154–1162.
(11) Sowa, T.; Kawamura, T.; Shida, T.; Yonezawa, T. *Inorg. Chem.* **1983**, *22*, 56–61.
(12) Norman, J.G.; Kolari, H.J. *J. Am. Chem. Soc.* **1978**, *100*, 791–799.
(13) Stranger, R.; Medley, G.A.; McGrady, J.E.; Garrett, J.M.; Appleton, T.G. *Inorg. Chem.* **1996**, *35*, 2268–2275.
(14) Sizova, O.V.; Ivanova, N.V. *Russ. J. Coord. Chem.* **2006**, *32*, 444–450.
(15) Sizova, O.V. *J. Mol. Struct. Theochem.* **2006**, *760*, 183–187.
(16) Frisch, M.J.; Trucks, G.W.; Schlegel, H.B.; Scuseria, G.E.; Robb, M.A.; Cheeseman, J.R.; Scalmani, G.; Barone, V.; Mennucci, B.; Petersson, G.A.; Nakatsuji, H.; Caricato, M.; Li, X.; Hratchian, H.P.; Izmaylov, A.F.; Bloino, J.; Zheng, G.; Sonnenberg, J.L.; Hada, M.; Ehara, M.; Toyota, K.; Fukuda, R.; Hasegawa, J.; Ishida, M.; Nakajima, T.; Honda, Y.; Kitao, O.; Nakai, H.; Vreven, T.; Montgomery, J.A. Jr.; Peralta, J.E.; Ogliaro, F.;

Bearpark, M.; Heyd, J.J.; Brothers, E.; Kudin, K.N.; Staroverov, V.N.; Kobayashi, R.; Normand, J.; Raghavachari, K.; Rendell, A.; Burant, J.C.; Iyengar, S.S.; Tomasi, J.; Cossi, M.; Rega, N.; Millam, N.J.; Klene, M.; Knox, J.E.; Cross, J.B.; Bakken, V.; Adamo, C.; Jaramillo, J.; Gomperts, R.; Stratmann, R.E.; Yazyev, O.; Austin, A.J.; Cammi, R.; Pomelli, C.; Ochterski, J.W.; Martin, R.L.; Morokuma, K.; Zakrzewski, V.G.; Voth, G.A.; Salvador, P.; Dannenberg, J.J.; Dapprich, S.; Daniels, A.D.; Farkas, Ö.; Foresman, J.B.; Ortiz, J.V.; Cioslowski, J.; Fox, D.J. *Gaussian 09*; Revision A.1, Gaussian, Inc. Wallingford, CT, 2009.

(17) Vlcek, A. Jr.; Zalis, S. *Coord. Chem. Rev.* **2007**, *251*, 258–287.

(18) Tozer, D.J.; Amos, RD.; Handy, N.C.; Roos, B.O.; Serrano-Andres, L. *Mol. Phys.* **1999**, *97*, 859–868.